REPORT DOCUMENTATION PAGE

Form Approved
OMB No. 0704-0188

PLEASE DO NOT RETURN YOUR FORM TO THE ABOVE ADDRESS.

1. REPORT DATE *(DD-MM-YYYY)*	2. REPORT TYPE	3. DATES COVERED *(From - To)*
11/10/2009	Final Performance Technical Report	04/29/2008-06/30/2009

4. TITLE AND SUBTITLE

Turbulence Parameterization and Lateral Mixing

5a. CONTRACT NUMBER

5b. GRANT NUMBER

N00014-08-1-0974

5c. PROGRAM ELEMENT NUMBER

6. AUTHOR(S)

Eric A. D'Asaro

5d. PROJECT NUMBER

5e. TASK NUMBER

5f. WORK UNIT NUMBER

7. PERFORMING ORGANIZATION NAME(S) AND ADDRESS(ES)

Applied Physics Laboratory, University of Washington
1013 N.E. 40th Street
Seattle, WA 98105

8. PERFORMING ORGANIZATION REPORT NUMBER

9. SPONSORING/MONITORING AGENCY NAME(S) AND ADDRESS(ES)

Theresa Paluszkiewicz, ONR 32
Office of Naval Research
875 North Randolph Street
Arlington, VA 22203-1995

10. SPONSOR/MONITOR'S ACRONYM(S)

11. SPONSOR/MONITOR'S REPORT NUMBER(S)

12. DISTRIBUTION/AVAILABILITY STATEMENT

UU

13. SUPPLEMENTARY NOTES

14. ABSTRACT

This project funded approximately one month of salary for the PI to prepare for and participate in an ONR workshop in Alaska, planning for the field programs in 2011 and 2012 as part of the ONR Lateral Mixing DRI. Meeting expenses included airfare and per diem. At the meeting, analysis results supported by a previous ONR grant, N00014-94-1-0024 were discussed with ONR Program Managers.

15. SUBJECT TERMS

16. SECURITY CLASSIFICATION OF:			17. LIMITATION OF ABSTRACT	18. NUMBER OF PAGES	19a. NAME OF RESPONSIBLE PERSON
a. REPORT	b. ABSTRACT	c. THIS PAGE			Eric D'Asaro
UU	UU	UU	UU	1	19b. TELEPHONE NUMBER *(Include area code)* 206-685-2982

Reset

Standard Form 298 (Rev. 8/98)
Prescribed by ANSI Std. Z39.18

Final Technical Report

Turbulence Parameterization and Lateral Mixing

Eric A. D'Asaro, Principal Investigator
APL/UW 1013 NE 40th Str, Seattle, WA 98105
phone: (206) 685-2982 fax: (206) 543-6785 email: dasaro@apl.washington.edu

Grant Number: N00014-08-1-0974

Performance Period: April 29, 2008 – June 30, 2009

This project funded approximately one month of salary for the PI to prepare for and participate in an ONR workshop in Alaska, planning for the field programs in 2011 and 2012 as part of the ONR Lateral Mixing DRI. Meeting expenses included airfare and per diem. At the meeting, analysis results supported by a previous ONR grant, N00014-94-1-0024 were discussed with ONR Program Managers.*

Dr. D'Asaro submitted a follow-on proposal for the Lateral Mixing DRI that was subsequently funded under ONR grant N00014-09-1-0172, performance period 1/1/09-12/31/11.

*D'Asaro, E. (2008), A diapycnal mixing budget on the Oregon shelf, Limnol Oceanogr. 53, 2137-2150.

Limnol. Oceanogr., 53(5, part 2), 2008, 2137–2150

A diapycnal mixing budget on the Oregon shelf

Eric A. D'Asaro[1]
Applied Physics Laboratory and Department of Oceanography, 1013 NE 40th Street, Seattle, Washington 98105

Abstract

Although isopycnal mixing is undoubtedly important at global and gyre scales, the relative importance of isopycnal and diapycnal mixing on much smaller scales is uncertain. This issue is investigated using 35 d of data from a Lagrangian float deployed on a mid-depth isopycnal on the Oregon shelf. Measurements of temperature, salinity, and pressure maintain the float on the isopycnal; its high-frequency diapycnal deviations are used to estimate the diapycnal diffusivity using an inertial subrange method; lower-frequency deviations, including intentional profiles to the surface, are used to estimate diapycnal derivatives near the target isopycnal. Downward irradiance at 490 nm is used to calibrate chlorophyll fluorescence measurements and compute solar heating rates. Corrections for the diapycnal deviations provide a nearly continuous isopycnal time series of spice (a temperature and salinity combination nearly orthogonal to potential density) and chlorophyll. A new formulation of the diffusion equation in isopycnal coordinates is derived and used to test the accuracy of purely diapycnal mixing balances for spice and chlorophyll. On vertical scales of about 10 m and timescales of about 2 d, isopycnal spice variations are mostly controlled by diapycnal mixing, although other processes, presumably isopycnal mixing, are sometimes important. Processes other than diapycnal mixing control isopycnal chlorophyll variations on these scales. Likely candidates include isopycnal mixing with a nearby bloom, planktonic sinking out of this bloom, or possibly local phytoplankton growth. Thus both isopycnal and diapycnal mixing can be important at these small scales.

Isopycnal mixing is clearly important to the large and mesoscale distribution of scalars in the ocean. Gyre circulations and mesoscale eddies stir the global-scale gradients in temperature and salinity to smaller scales. On these large scales the flow is nearly adiabatic and the stirring is therefore nearly isopycnal. Both models and data suggest that such stirring moves scalar variance down to at least kilometer scales (Sundermeyer and Price 1998). Diabatic mixing removes this variance on smaller scales. In models, this is often done by isopycnal or horizontal diffusivity, but it is not known whether isopycnal or diapycnal mixing dominates in the real ocean. Process studies of ocean mixing have concentrated almost exclusively on diapycnal mixing at scales of meters to millimeters. Established techniques for the estimation of diapycnal mixing using microstructure measurements rely on diapycnal (or vertical) variance balances (Gregg 1987; Thorpe 2005) with little reference to the possibility of isopycnal processes playing an important role. One possibility is that the flux of scalar variance from large to small scale occurs isopycnally at large scales and diapycnally at microscales, with the transition scale being in the poorly measured range between meters and kilometers. If so, then the local Lagrangian rates of change, i.e., the turbulent flux divergences, would be balanced diapycnally when viewed at meter scales, but isopycnally when averaged over larger scales. In this paper, the relative importance of isopycnal and diapycnal mixing at meter scales is tested by comparing the Lagrangian rate of change of the scalar "spice," a combination of temperature and salinity that represents water mass properties, with the divergence of the diapycnal flux of spice. A similar test is made for chlorophyll concentration. The following sections describe the theoretical approach, the instrumentation and data processing, the tests, and their interpretation.

Techniques

Mixing rates from an isopycnal budget—McDougall's analysis: Consider an "isopycnal" float, i.e., a float that moves horizontally with the velocity of the water and moves vertically to remain on a surface of constant potential density referenced to the surface, $\sigma(S,T,P)$, with value σ_0. The equation for the rate of change of a scalar C measured on the float is

$$\frac{DC}{D_t} \equiv C_t = -(e - \mathcal{D}_d)C_d + \mathcal{D}C_{dd} + \nabla_i \cdot K \nabla_i C + Q^c \quad (1)$$

where the subscript d implies a diapycnal partial derivative, ∇_i is an isopycnal horizontal gradient operator, $\mathcal{D}$ is the diapycnal diffusivity, K is the isopycnal diffusivity, and e is the diapycnal velocity, i.e., the velocity across or through the isopycnal surface. Other sources of C, for example, solar heating for a temperature budget, are represented by Q^c. The actions of e and $\mathcal{D}_d$ cannot be distinguished in budget calculations. Accordingly, an effective diapycnal advective velocity is defined as

$$\tilde{e} \equiv e - \mathcal{D}_d \quad (2)$$

[1] Corresponding author (dasaro@apl.washington.edu).

Acknowledgments

Trevor McDougall originally suggested this approach. Thanks to Eric Rehm and Rick Reynolds for help with optical modeling, and to anonymous reviewers who improved the paper. This work was made possible by support from the APL-UW Ocean Engineering Department, especially Michael Ohmart and Michael Kenney.

This work was supported by ONR grant N00014-94-1-0024.

McDougall (1984) takes these equations for θ and S with $Q^\theta = 0$ and $Q^S = 0$, eliminates $\tilde{e}$, and uses the relationship (his equation 6)

$$S_{\theta\theta} = \frac{\theta_{dd} S_d}{\theta_d^3}\left(\frac{\theta_d}{S_d}\frac{S_{dd}}{\theta_{dd}} - 1\right) \quad (3)$$

to derive

$$\theta_t = \mathcal{D} g N^{-2} \theta_d^3 \beta S_{\theta\theta} + K\left(\nabla_i^2 \theta + N.L.\right) \quad (4)$$

relating the rate of change of temperature measured by an isopycnal float to the diffusivities and thermohaline structure. Here β is the haline contraction coefficient $\beta = \rho^{-1}\partial_s \rho|_{\theta,P}$ and N is the buoyancy frequency.

In general, both the diapycnal and isopycnal diffusivity can change the temperature. Isopycnal mixing also acts through the nonlinearity of the equation of state to contribute the terms labeled "N.L." These are described more fully in McDougall (1984). For $K = 0$, there is a direct relationship between θ_t and $\mathcal{D}$, which depends on the curvature of the T/S relationship $S_{\theta\theta}$. Practically, however, there are problems with Eq. 4. Its form is not intuitive and $S_{\theta\theta}$ can be zero, infinite, or even multivalued. Accordingly, an alternative form is sought.

The spice variable Π: Potential density can be expanded locally in terms of β and α, the thermal expansion coefficient, as

$$\sigma(S,\theta) = \sigma(S_0,\theta_0) - \alpha(\theta - \theta_0) + \beta(S - S_0) \quad (5)$$

Flament (2002) defines spiciness (abbreviated here as spice), denoted by $\Pi(S, \theta)$, as the natural companion to potential density $\sigma(S, \theta)$. The units of σ and Π are the same and Π is defined to be zero at $\theta = 0$, salinity $(S) = 35$. Locally, Π is expanded as

$$\Pi(S,\theta) = \Pi(S_0,\theta_0) + \Pi_\theta(S_0,S_0)\left[(\theta - \theta_0) + \frac{\beta}{\alpha}(S - S_0)\right] \quad (6)$$

where Π_θ is the partial derivative of Π with respect to θ and the defining relationship $\beta\Pi_\theta = \alpha\Pi_S$ has been used. The exact definition within these constraints is formed requiring Π to be minimally correlated with σ over the range of oceanic water masses.

In general, Π is not a linear function of θ and S because α and β are functions of θ and S. Therefore, like $\sigma_{\theta,}$ Π is, in general, not conserved during mixing. These effects will be ignored in this paper and the full nonlinear, nonconservative form of the Flament (2002) Π will be used. However, parallel computations using a linearized, conservative form of Π were also made, as described in the section "Mixing budgets." The differences are negligible.

An isopycnal equation for Π: If depth and temperature deviations are small, the deviations of the equation of state from Eqs. 5 and 6 should be small. Applying Eq. 1 to θ and S with $K = 0$ and using Eq. 5 yields an equation for σ

$$\frac{D\sigma}{Dt} = -\tilde{e}\sigma_d + \mathcal{D}\sigma_{dd} - \alpha\sigma Q \quad (7)$$

where Q, with no superscript, is the local rate of heating in units of θ_t [°C s^{-1}]. Because the measurements are along an isopycnal,

$$\frac{D\sigma}{Dt} = 0 \quad (8)$$

so that

$$\tilde{e} = \mathcal{D}\frac{\sigma_{dd}}{\sigma_d} - \alpha\sigma\frac{Q}{\sigma_d} \quad (9)$$

requiring curvature of the density profile or local heating or cooling to produce a diapycnal velocity. The equivalent equation for Π is

$$\frac{D\Pi}{Dt} = -\tilde{e}\Pi_d + D\Pi_{dd} + \Pi_\theta Q \quad (10)$$

A diagnostic equation: Equations 9 and 10 can be solved for $\mathcal{D}$

$$\Pi_t = \mathcal{D}\Pi_{dd}\left(1 - \frac{\Pi_d}{\sigma_d}\frac{\sigma_{dd}}{\Pi_{dd}}\right) + Q\left(\Pi_\theta + \alpha\sigma\frac{\Pi_d}{\sigma_d}\right) \quad (11)$$

The right two terms are the usual diffusion equation with a source, but with the addition of the extra factors in parentheses resulting from diapycnal advection due to diapycnal diffusion. Diffusion moves the isopycnal through the water. These extra factors quantify this effect.

For this analysis, it will be easier to take σ derivatives than diapycnal derivatives. Therefore $\Pi = \Pi(\sigma)$ will be assumed for the purpose of evaluating the right side of Eq. 11. Obviously this cannot be exactly true if Π_t is nonzero on an isopycnal, so it cannot be assumed otherwise. Using the chain rule to express Π_d and Π_{dd} in terms of σ derivatives yields

$$\Pi_t = \mathcal{D}\Pi_{\sigma\sigma}\sigma_d^2 + Q(\Pi_\theta + \alpha\sigma\Pi_\sigma) \quad (12)$$

or in more conventional notation

$$\frac{D\Pi}{Dt} = \mathcal{D}\frac{\partial^2\Pi}{\partial\sigma^2}\frac{\rho^2 N^4}{g^2} + Q\left(\frac{\partial\Pi}{\partial\theta} + \alpha\sigma\frac{\partial\Pi}{\partial\sigma}\right) \quad (13)$$

This can be used to estimate the diapycnal diffusivity

$$\mathcal{D}_\Pi = \frac{\hat{\Pi}_t}{\Pi_{\sigma\sigma}\sigma_d^2} \quad (14)$$

where $\mathcal{D}_\Pi$ is the diffusivity computed using Eq. 14 and

$$\hat{\Pi}_t = \Pi_t - Q(\Pi_\theta + \alpha\sigma\Pi_\sigma) \quad (15)$$

is Π_t corrected for solar heating. These expressions contain the same physics as Eq. 4 with the addition of the heating term, but are written in terms of diapycnal derivatives instead of θ and S derivatives. The change in properties along the isopycnal due to diapycnal mixing depends on the curvature of the Π–σ diagram and the stratification. However, the form is much simpler, and thus easier to evaluate, and the curvature is always well defined.

Scalar changes: A similar analysis applies to the rate of change of any scalar. From Eq. 1 using Eq. 9:

$$C_t = \mathcal{D}\left[C_{dd} - \frac{\sigma_{dd}}{\sigma_d} C_d\right] + \alpha Q \frac{C_d}{\sigma_d} Q^c \tag{16}$$

Again assuming $C = C(\sigma)$ and using the chain rule

$$C_t = \mathcal{D} C_{\sigma\sigma} \sigma_d^2 + \alpha \sigma Q C_\sigma + Q^c \tag{17}$$

which, not surprisingly, is a slightly more general form of Eq. 12.

Budget method summary: Equation 12 or 17 describes the local budget for scalars Π or C in an isopycnal coordinate system moving with the water. Because water moves across isopycnals in the presence of mixing, this is different from a fully Lagrangian coordinate system because of the diapycnal velocity $\tilde{e}$. The value of $\mathcal{D}$ can be estimated by these equations assuming no isopycnal mixing. The diapycnal velocity $\tilde{e}$ is implicit in the calculation, but can be evaluated from Eq. 9 if the gradient of stratification N_d^2 is known. Here, the strategy is to compare the value of $\mathcal{D}$ estimated in this way with microscale estimates and thereby test the assumption that $K = 0$.

Diapycnal mixing from microscale measurements—The Osborn and Cox (1972) method computes the down-gradient flux of any scalar from its dissipation rate and its gradient. Winters and D'Asaro (1996) show that this formula is exact if the correct definition of diapycnal gradient is used. Evaluation of the difference between their definition and the usual spatial gradient using density fields from numerical simulations (D'Asaro et al. 2004) and ocean data shows that there is little difference. Applying this to potential density σ, so as to yield the diapycnal diffusivity of potential density, yields

$$\mathcal{D}_\chi = -\frac{\chi}{2\left(\frac{\partial \sigma}{\partial z}\right)^2} = \chi \frac{g^2}{2N^4 \rho^2} \tag{18}$$

The dissipation rate of potential density variance χ was estimated as in D'Asaro and Lien (2007). In a turbulent fluid Lagrangian frequency spectra of scalars $\Phi_\sigma(\omega)$ exhibit an inertial subrange for Lagrangian frequencies ω above about N. This corresponds to the $-5/3$ spectrum found for scalar wave number spectra (Sreenivasan 1996), but here found for frequency instead of wave number. D'Asaro and Lien (2007) show that this spectrum should have the form

$$\Phi_{\frac{D\sigma}{Dt}}(\omega) = \beta_s \chi \tag{19}$$

It is white and proportional to the dissipation rate for the scalar. The value of the Kolmogorov constant $\beta_s = 0.6$ has an uncertainty of less than a factor of two. In principle, then, χ can be estimated directly from the level of the spectrum of the Lagrangian rate of change of potential density $\Phi_{\frac{D\sigma}{Dt}}$ within the inertial subrange.

Practically, the finite size of real floats leads to deviations of the spectral forms from Eq. 19. Observed spectra in D'Asaro and Lien (2007) collapse to a single nondimensional form

$$\Phi_{\frac{D\sigma}{Dt}}(\omega) = \beta_s \chi H(\omega/\omega_L) = \beta_s \chi \left[1 + \frac{\omega}{3.0\omega_L} + \left(\frac{\omega}{4.5\omega_L}\right)^2\right] \tag{20}$$

where H is an empirical nondimensional function, increasing at high frequencies because of advection of density fluctuations past the float's density sensor. Here

$$\omega_L = \left(\varepsilon/L^2\right)^{1/3} \tag{21}$$

is the frequency at which the float size L becomes important. The value of χ is estimated from the average value of $\Phi_{\frac{D\sigma}{Dt}}(\omega)/\beta_s H(\omega/\omega_L)$ for $\omega < 2\omega_L$ (D'Asaro and Lien 2007).

The dissipation rate of kinetic energy ε, needed in Eq. 21, was evaluated by equating Eq. 18 with the Osborn (1980) formula

$$\mathcal{D}_\varepsilon = \Gamma \frac{\varepsilon}{N^2} \tag{22}$$

relating the diapycnal diffusivity to ε in terms of a "mixing efficiency" Γ, taken to be 0.2 (Gregg 1987). Lien et al. (1998) and Lien and D'Asaro (2006) describe a method to compute ε from the Lagrangian spectra of vertical acceleration $\Phi_a(\omega)$ measured by a Lagrangian float. Here, however, the high noise level of the pressure sensor prevents this method from being used except in a very few cases.

For very weak mixing this method will fail as the inertial subrange disappears. The numerical study of D'Asaro et al. (2004) suggests that this limit is reached at values of ε below 10^{-9} W kg^{-1}, equivalent here to values of $\mathcal{D}_\chi$ below about 10^{-6} m^2 s^{-1}.

A consistency test—Using $\mathcal{D}_\chi$ from Eq. 18 in Eq. 12 yields the simple expression

$$\hat{\Pi}_t = \frac{\chi}{2} \Pi_{\sigma\sigma} \tag{23}$$

If mixing is entirely diapycnal Eq. 23 should be true. Deviations indicate either a significant isopycnal flux divergence or problems with either the budget or microstructure methods. Using Eq. 23 is a better test for diapycnal balance than directly comparing $\mathcal{D}_\chi$ with $\mathcal{D}_\Pi$ because it does not require dividing by $\Pi_{\sigma\sigma}$, a quantity that can be zero, and because it eliminates N from the calculation.

Data and analysis

The Lagrangian float—The analysis will use data from a single Lagrangian float, MLFII (mixed-layer float, second generation) number 8 since this was the only float measuring chlorophyll. The float profiled every 12 h from a depth of 40–60 m to the surface. Between profiles, i.e., during "drifts," it actively adjusted its buoyancy to remain near the 25.5 kg m^{-3} isopycnal. The float position was determined at the top of some profiles using system

ARGOS because the global positioning system (GPS) did not function. The float measured pressure, temperature, salinity (Seabird 41CT), downwelling irradiance at 490 nm (Biospherical Instruments QCP200), and chlorophyll fluorescence (Wetlabs ECO) every 100 s during drifts and with roughly 1-m resolution during profiles. Details on these floats can be found in D'Asaro (2003). Details on their measurements of the subinertial and internal wave environments on the Oregon shelf can be found in D'Asaro (2004) and D'Asaro et al. (2007).

The float was deployed on 23 July 2001 (day 205.62) at about 45.5°N at the 100-m isobath (Fig. 1). The float traveled south in the prevailing current, moving offshore and stalling near the shelf break on days 210–215, then moving more rapidly across Heceta Bank by day 220. During this time the target isopycnal remained at 20–40 m. On about day 230, the float moved offshore near Cape Blanco and descended, with the isopycnal, to a depth of about 50 m. The mission continued through day 275, but this latter, offshore part of the trajectory is not considered here.

During the "drift" periods between profiles, these floats are Lagrangian at high frequencies and isopycnal at low frequencies (D'Asaro 2003). At low frequencies they dynamically adjust their volume in response to the measured T, S, and P so that the float measures a constant potential density and therefore remains on an isopycnal surface. At high frequencies they are Lagrangian, i.e., they follow the three-dimensional motion of the water. The transitional frequency between Lagrangian and isopycnal behavior is about $N/30$; the additional drag of the large horizontal cloth drogue decreases this frequency to well below N.

Bio-optical models—Scope: This section describes the calibration of the irradiance and chlorophyll fluorescence sensors and the models used with these data to estimate the rate at which solar radiation heats the water.

Radiometer calibration: The Biospherical QCP200 measured downwelling irradiance at 490 nm. This was checked by pointing the sensor upward at a clear blue sky on 1939Z 11 July 2001. Using the manufacturer's calibration, the sensor measured $E_{490} = 1.64$ W m^{-2} nm^{-1}. At the same time a shortwave radiometer about 1 km away, corrected for aging (D'Asaro 2007), measured a total shortwave radiation $E_{sw} = 911$ W m^{-1}. The online version of the coupled ocean and atmosphere radiative transfer (http://snowdog.larc.nasa.gov/jin/rtset.html) (Jin et al. 2006) was used with the following parameters: visibility 140 km (from Puget Sound Clean Air Agency), integrated ozone amount = 325 Dobson units (DU) (from Environment Canada, ftp://es-ee.tor.ec.gc.ca/pub/ozone_maps/nh/), a "mid-latitude summer" atmospheric model, a "MODTRAN Maritime" or "OPAC Continental Clean" mixed layer model, no clouds, and a total precipitable water = 3.15 g cm^{-2} tuned to yield the observed E_{sw}. This yielded $E_{490} = 1.64$ W m^{-2}, about 3% smaller than that measured. This is within the expected errors in radiometer calibration.

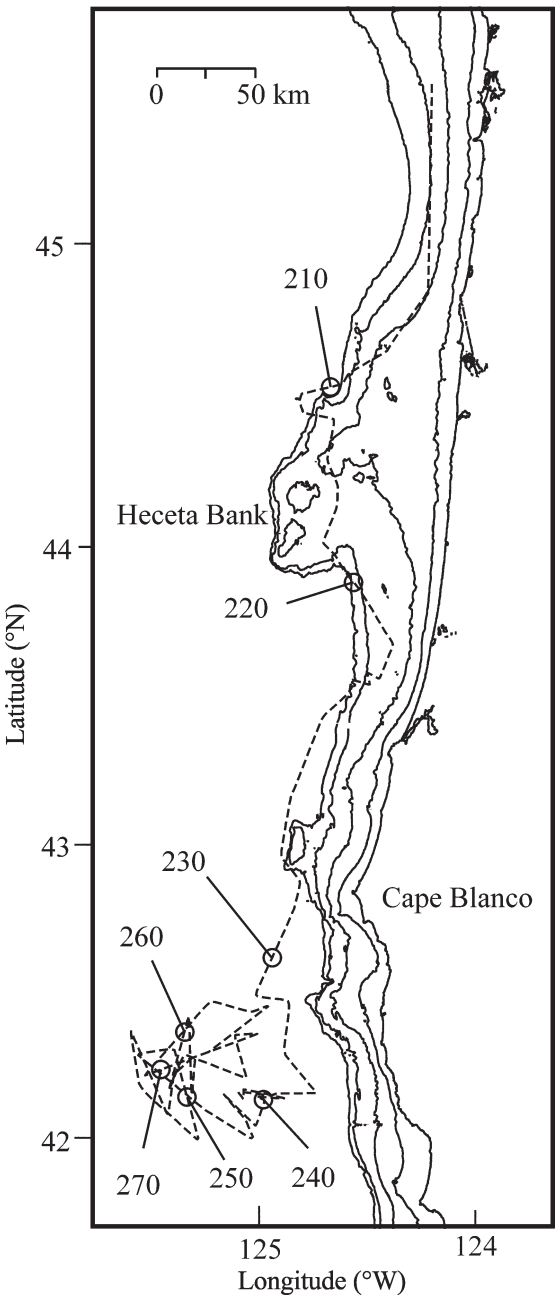

Fig. 1. Track of float 8 (dashed line) overlaid on topography of Oregon shelf. Isobaths at 50, 100, 150, and 200 m are shown. Time is labeled along the track; every 10th day of the year 2001 is shown.

Diffuse attenuation profile: Vertical profiles of irradiance E_{490} were made twice daily, near 5Z and 17Z. The 5Z profiles occurred nearly at sunset for the first part of the mission. Later, they occurred after dark and were not useful. The 17Z profiles occurred during mid-morning with a solar elevation near 30°. As can be seen in Fig. 2, a complete profile often required using both the up and down casts. Typically, however, the irradiance from the up and down profiles did not match, presumably because the surface irradiance changed during the approximately 1-h interval between them. Because the shapes were usually

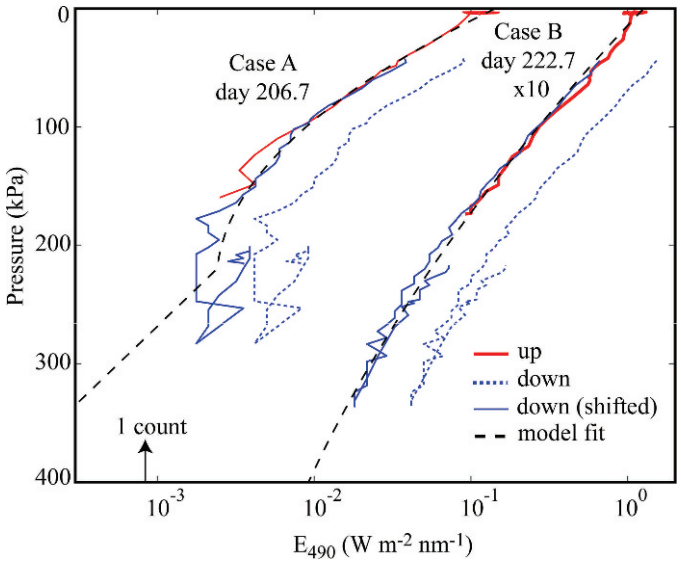

Fig. 2. Two typical irradiance profiles. In each, the upward-going segment (red) is offset from downward-going segments (blue, dotted line) occurring about 1 h later. These are merged into a single profile by multiplying the downward segment by an appropriate factor (blue solid line). This works well in case B, less well for case A. The black dashed line shows the fit of Eq. 24 to the combined profile and, for case A only, an extension to very low light level using Eq. 25. The profile for case B is shifted by a factor of 10 so that it does not overlap the profile from case A. The irradiance level equivalent to one count is indicated. The length of the vertical axis on this plot is 400 kPa, which is approximately equal to 40 m.

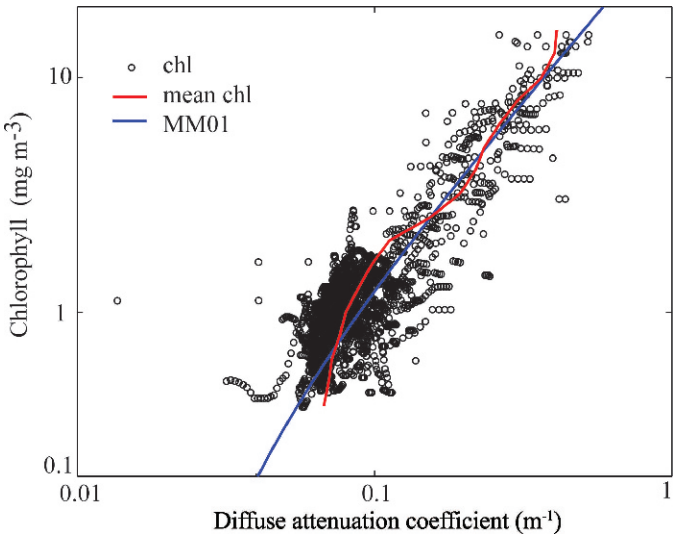

Fig. 3. Scatter plot of K_{490} and calibrated chlorophyll high light level (dots). Blue line is the Morel and Maritorena (2001) relationship. Red line shows the values of K_{490} averaged in chlorophyll bins.

very similar, the two profiles were combined by shifting the down profile to match the up profile using a factor determined for each profile by eye. Only profiles with at least 10 data points, a maximum depth of at least 5 dbar, and a maximum irradiance of at least 50 counts were used. Data points with less than three counts were excluded from the analysis. The combined profile was fit with a log-quadratic function

$$E_{490} = E_q e^{-c_1 P - c_2 P^2} \tag{24}$$

and with a linear form

$$E_{490} = E_0 e^{-c_3 P} \tag{25}$$

A complete irradiance profile was constructed using Eq. 24 at all depths where this form decreased with depth, occasionally extending the profile below this depth using the constant value of K_{490} from Eq. 25.

Two sample profiles and fits are shown in Fig. 2. The combined profiles are accurately fit by Eq. 24 for case B. For case A, however, K_{490} is sufficiently large that the light level falls below the sensitivity of the instrument within the profile. This, and the variability of the surface illumination with time, results in a cusp in the irradiance curve at depth. This could probably be eliminated by more careful analysis, but the light levels are so low that these details have little effect on water column heating, the goal of this analysis.

Fluorometer calibration: The Wetlabs ECO fluorescence reading F was converted to chlorophyll using the Morel and Maritorena (2001) empirical relationship for type 1 waters between chlorophyll concentration Chl [mg m^{-3}] and the diffuse attenuation coefficient at 490 nm K_{490} [m^{-1}]

$$K_{mm} = 0.01660 + 0.07242 Chl_{mm}^{0.68955} \tag{26}$$

This method is insensitive to changes in the irradiance sensor calibration due to biofouling because K_{490} depends only on the ratios of irradiance with depth, not the absolute irradiance.

The fluorescence data show large increases beginning about day 235. The increases were rarely found during down profiles, but were common during up profiles, suggesting that they were due to a piece of plant attached to the float that was swept upward, out of view of the fluorometer, during down profiles. The increases were removed from the profile data by deleting all data from up profiles, which was more than a factor of two larger than the data from down profiles interpolated to its location. The analysis shown here ends on day 240, so these artifacts have little effect.

Figure 3 shows the calibrated Chl, computed using $Chl = a + bF$, plotted against Chl_{mm}. The constants a and b were adjusted to provide a good fit. Only data for which $E_{490} > 8 \times 10^{-3}$ Wm^{-2} nm^{-1} (symbols) are plotted in Fig. 3 and used as data because smaller values do not correlate well. The average accuracy of the calibration, given by the standard deviation of $<K>/K_{mm}$, where $<K>$ is K_{490} averaged in Chl bins (white circles) and K_{mm} is the Morel and Maritorena (2001) value of K_{490} for each bin, is 11%.

Radiation fields and heating rate: The model irradiance profiles (e.g., Fig. 2) were interpolated to compute the ratio $E_{490}(0)/E_{490}(Z_f)$ of irradiance at the surface and at the float

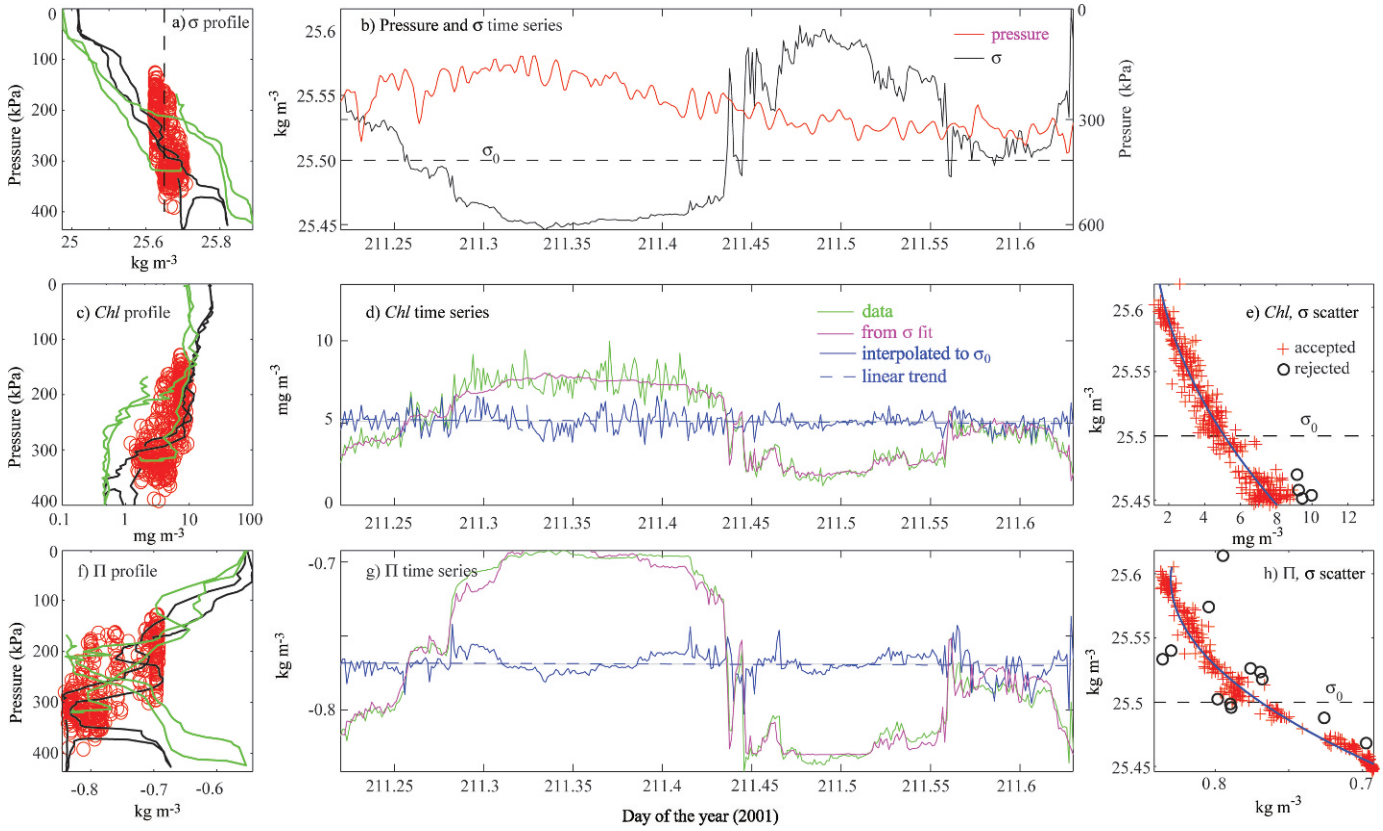

Fig. 4. Isopycnal analysis for drift segment 12, a segment with an especially large diapycnal correction. Profiles of (a) potential density σ, (c) chlorophyll, and (f) spice Π from before (black) and after (green) this drift segment. Red circles show data during drift. Time series during drift of (b) pressure (red solid line, 400 kPa = 40 dbar) and σ (black solid line), (d) chlorophyll (green), and (g) Π (green). Scatter plots of (e) *Chl* and (h) Π against σ during the drift. A least-squares quadratic fit (blue line) is computed after recursively rejecting data deviating by more than 3 SD from fit. Rejected data are plotted in black. These quadratic functions are used to predict $Chl(\sigma\,[t])$ and $\Pi\,(\sigma\,[t])$ (magenta) in panels d and g, respectively, and to compute their values at the target isopycnal (blue) Chl_0 and Π_0 in panels d and g, respectively. The rate of change of Chl_0 and Π_0 is computed from a least-squares line (blue dashed lines in panels d and g, respectively). Target isopycnal σ_0 is shown in panels b, e, and h (black dashed line).

depth. This, times the measured $E_{490}(Z_f)$, yields a nearly continuous estimate of $E_{490}(0)$ except at times when $E_{490}(Z_f)$ is so small that reliable estimates cannot be made. Because the heating at these times is also very small, the large relative errors are not important.

The full visible spectrum (200–700 nm) of downward irradiance at the surface, $E_\lambda(0)$, was computed from $E_{490}(0)$ using the spectral shape shown in fig. 74 of Jerlov (1976). The shortwave irradiance above the surface is estimated from the integral of $E_\lambda(0)$, with the addition of a 60% infrared component, i.e., $E_{sw} = \int E_\lambda(0)d\lambda/0.6$. This time series was compared with the data from shortwave radiometers on a mooring (Boyd et al. 2002) on the central Oregon shelf (44°59.757′N, 124°6.998′W). Two radiometers on the mooring differed by 5%; one was corrected to the other. The float time series tracks well both the daily cycle of irradiance and the variability between days as measured on the mooring. Obvious errors occur when the float is very dark, with some differences undoubtedly related to the geographic separation of the float and mooring.

During days 222–240 $E_{490}(Z_f)$ was above the noise level; the average values of E_{sw} from the mooring and the float differed by only 5% despite being separated by up to 250 km. This suggests that the float-based estimate of E_{sw} is accurate to 5–10%.

The surface spectrum $E_\lambda(0)$ was propagated downward using the Morel and Antoine (1994) empirical expressions for K_λ as a function of *Chl*. The total downgoing irradiance $E_d(t,z)$ was computed from the integral of the spectrum and the local heating rate $Q(t,z)$ from its change with depth. The heating at 490 nm $Q_{490}(t,z)$ was also computed. Their ratio $R_{490} = \mathrm{Q} / \mathrm{Q}_{490}$ was computed as a function of depth and time with a resolution of about 1 d. A time series $Q_{490}(Z_f) = E_{490}(Z_f)K_{490\mathrm{mm}}(Chl\,[Z_f])$ was measured at the float at much higher time resolution. The heating rate at the float at high resolution was thus estimated as $Q(t) = Q_{490}(Z_f[t])\mathrm{R}_{490}(t,Z_f)$.

Mixing budgets

Methods—The analysis here is focused on evaluating the terms in Eqs. 12, 23, and 17 along the $\sigma_0 = 25.5$ kg m^{-3} isopycnal. Analysis was conducted separately for each approximately 9.8-h-long (35.4 ks) "drift." An example is shown in Fig. 4. The float moved vertically about 20 m and diapycnally about 0.15 kg m^{-3} during this segment

(Fig. 4a,b). The measured chlorophyll and spice time series (Fig. 4d,g, green) show variations that are in phase with the σ fluctuations as shown by the tight lines in scatter plots (Fig. 4e,h) of *Chl* and Π against σ. Least-squares quadratic fits were made to these relationships (blue lines). For spice, let $\Pi_q(\sigma)$ be the least-squares quadratic fit from Fig. 4h. This predicts a variation $\Pi_D(t) = \Pi_q(\sigma[t])$ due to the diapycnal motion of the float alone. This is plotted as the magenta line in Fig. 4g, with a corresponding *Chl* plot in Fig. 4d. As expected $\Pi_D(t)$ and $Chl_D(t)$ account for much of the measured variability. This is removed by computing $\Pi_0(t) = \Pi(t) - \Pi_D(t) + \Pi_q(\sigma_0)$, the blue line in Fig. 4g, with a corresponding $Chl_0(t)$ in Fig. 4d. These have much less variability. They will be interpreted as a time series of Π and *Chl* at the σ_0 isopycnal.

The average rate of change on the isopycnal, i.e., Π_t and C_t in Eqs. 12 and 17, was computed for each segment from the slope of a least-squares fit line to $\Pi_0(t)$ and $Chl_0(t)$, respectively. The error in this estimate was computed by assuming that the data are the sum of this line and random correlated noise with a correlation function similar to the average correlation function estimated from the data. Random realizations of this model were computed and confidence limits computed from the distribution of the slope of the lines fit to these realizations. Notice that $\Delta_L\Pi = \int_{t_1}^{t_2} \Pi_t dt$, the integrated changes on the isopycnal, is not the same as $\Delta_F\Pi = \Pi(t_2) - \Pi(t_1)$, the total change along the float trajectory, because the float moves horizontally during the profiling and makes surface communications between each drift. Thus each drift can be considered a separate 9.8-h-long Lagrangian experiment starting at a different horizontal location on the isopycnal. $\Delta_L\Pi$ measures the cumulative changes from these experiments, ignoring the changes due to the location jumps between experiments. D'Asaro (2004) discusses the magnitude of these jumps in more detail.

The quantities $\Pi_{\sigma\sigma}$ and $C_{\sigma\sigma}$ are computed similarly. For each segment, all data, both drifts and profiles, extending from the center of the preceding segment to the center of the following segment and within $\delta\sigma$ of σ_0 are fit with a fourth-order polynomial in σ and the derivatives evaluated at σ_0. As will be discussed below, three values of $\delta\sigma$ from 0.2 to 0.3 kg m^{-3} were used; smaller values lead to a large uncertainty, and include a domain that is too far away from the target isopycnal. The error in $\Pi_{\sigma\sigma}$ is large and difficult to estimate as there is no good understanding of the statistics of meter-scale Π variations. An error was estimated by making separate polynomial fits for the first and second halves of each segment. The standard error was taken as the absolute value of the difference between these two estimates.

The stratification N for each float drift is taken from D'Asaro et al. (2007) (their fig. 4a). The float has only a single conductivity–temperature–depth (CTD) sensor so continuous measurements of stratification are not available. Values of N taken from the twice-daily profiles, e.g., Fig. 4a, are highly variable and do not yield accurate results. D'Asaro et al. (2007) instead use the high-frequency cutoff of the internal wave spectrum to compute a robust average N for each drift segment. The typical difference between this estimate and the CTD-based estimate for the one float for which this is available is 30%.

The spice budget—Figure 5 shows the diapycnal mixing budget for Π. The float drifted at 10–30-m depth (Fig. 5a) until day 234, when it dove to 40–60-m depth. Within each drift, its depth fluctuated over a 10–20-m range because of internal waves. However, relative to the target isopyncal σ_0 = 25.5 kg m^{-3} (Fig. 5b), the fluctuations are much less, only a few meters. The profiles (red curves in Fig. 5a) map out the variations in Π surrounding σ_0 as shown in Fig. 5b. The target isopycnal is near a minimum in Π, a cold, fresh layer most likely a remnant of the deep winter mixed layer. The layer persisted until the float passed into a different water mass on day 234. During this time Π_t is positive, consistent with diffusive warming of the layer (Fig. 5d). A small correction for solar heating (pink lines) makes little change. The strong curvature of Π near its minimum results in a positive value of $\Pi_{\sigma\sigma}$ (Fig. 5e). The dissipation rate of potential density variance χ and the diffusivity $\mathcal{D}_\chi$ computed from it (Fig. 5f) vary over two orders of magnitude. Equation 23 predicts similarly large variations in the rate Π_t at which diapycnal diffusion erases the cold fresh intrusion (Fig. 5g). The measured Π_t mostly tracks these variations well within the uncertainties. Thus a diapycnal mixing balance applies most of the time. A detailed discussion of the comparison is deferred to the next section.

This calculation depends on the choices of time and space averaging. Given the float sampling scheme, the natural timescale is the drift duration. However, averaging over about four such intervals, about 1.8 d, is necessary to reduce the noise. For a diffusivity of 10^{-4} (10^{-5}) m^2 s^{-1}, this corresponds to a diapycnal scale of 4 m (3 m) and, for N = 0.015 s^{-1}, a density difference of $\Delta\sigma$ = 0.1(0.07) kg m^{-3}. However, values of $\Pi_{\sigma\sigma}$ computed over density ranges this small are quite noisy; the larger values of $\Delta\sigma$ used in Fig. 5 produce more stable results, but may also introduce a bias in the value of $\Pi_{\sigma\sigma}$.

The relatively good match between the two estimates of Π_t in Fig. 5g was achieved only by increasing the value of β_s to 1.0 from the D'Asaro and Lien (2007) value of 0.6. This increased the estimated value of χ by a factor of 1.6. The change is well within the current uncertainty in β_s and could represent a more accurate estimate of its value. However, it could also be due to a low bias in the estimate of $\Pi_{\sigma\sigma}$.

The effect of using a nonlinear and thus nonconservative Π in these calculations was assessed by defining a new spice function for each drift segment of the analysis, linearized around the mean values S_0 and θ_0 for that segment,

$$\hat{\Pi}(S,\theta) = \Pi(S_0,\theta_0) + \Pi_S(S_0,\theta_0)[S - S_0] + + \Pi_\theta(S_0,\theta_0)[\theta - \theta_0] \quad (27)$$

where Π_S and Π_θ are the partial derivatives of Π. Figure 5g shows the results of using $\hat{\Pi}(S,\theta)$ instead of $\Pi(S,\theta)$ using a dimmed version of the same lines. These two different computations are barely distinguishable, showing that the use of a conservative Π has little effect.

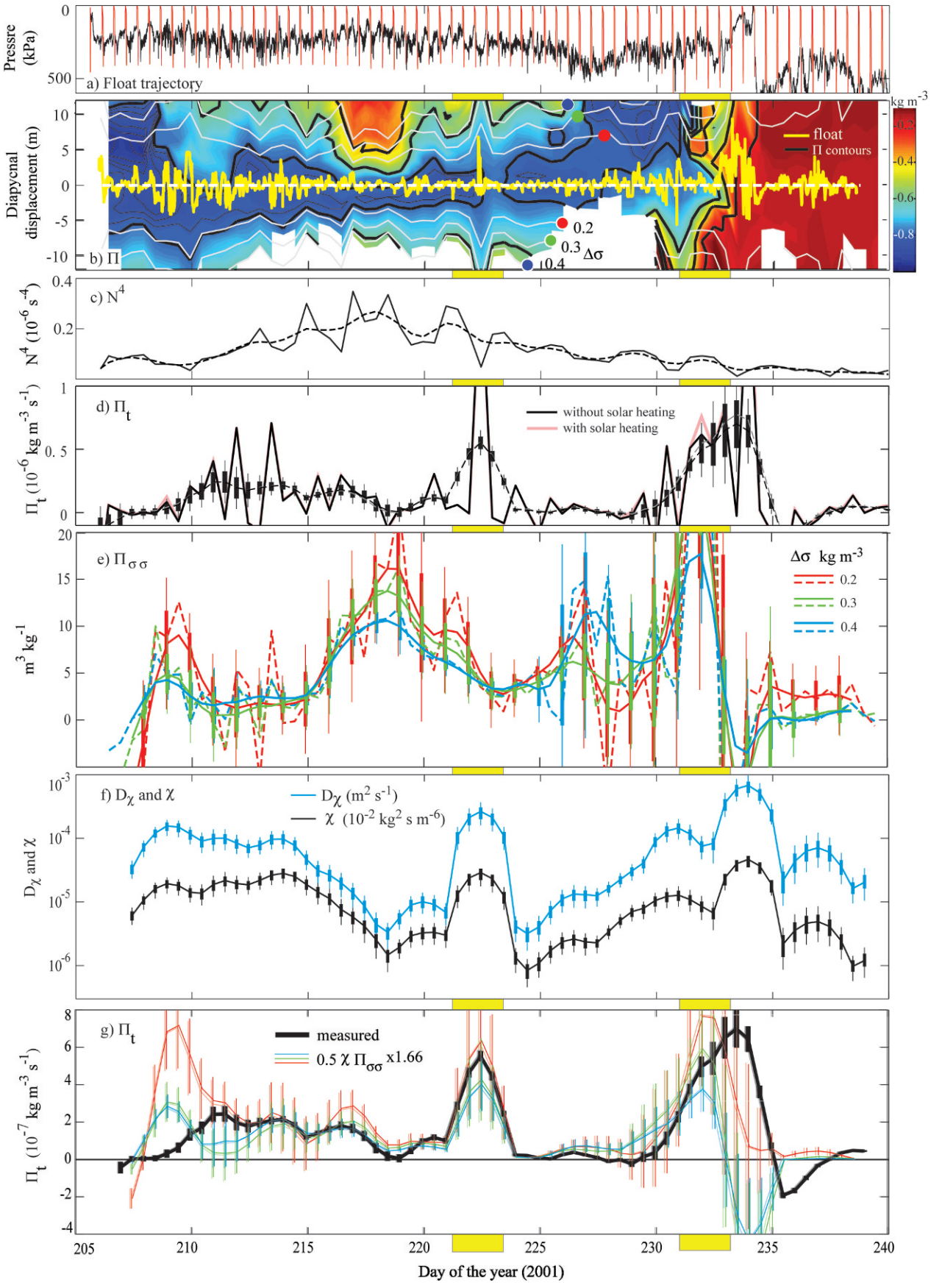
Pressre (kPa)
a) Float trajectory
Diapycnal displacement (m)
b) Π
float
Π contours
kg m-3
0.2
0.3
0.4
Δσ
c) N4
N4 (10-6 s-4)
d) Πt
without solar heating
with solar heating
Πt (10-6 kg m-3 s-1)
e) Πσ σ
Δσ kg m-3
m3 kg-1
f) Dχ and χ
Dχ (m2 s-1)
χ (10-2 kg2 s m-6)
g) Πt
measured
0.5 χ Πσσ x1.66
Πt (10-7 kg m-3 s-1)
Day of the year (2001)

An intense mixing event—A striking feature in the data is the intense mixing event on day 222, examined in detail and at maximum resolution in Fig. 6. Spectra of $\frac{d\sigma}{dt}$ (Fig. 6a) show a spectral level during the drift segment centered on day 222.4 about 25 times larger than the average value in the four nearby segments. Assuming $\beta_s = 0.6$ and $\Gamma = 0.2$, this spectrum implies $\varepsilon = 9 \times 10^{-7}$ m^2 s^{-3}, a diapycnal diffusivity $\mathcal{D}_\chi = 9 \times 10^{-4}$ m^2 s^{-1} averaged over the $T =$ 10.8-h-long segment, and a mixing thickness $(\mathcal{D}_\chi T)^{0.5}$ of about 6 m. A partial homogenization of the water column over a depth of 5–10 m is seen by the reduced N (Fig. 5c) and the reduced minimum in Π (Figs. 5b, 6e) extending for about 1 d after the event.

This mixing is intense enough to allow a second estimate of the mixing rate to be made using the acceleration spectrum (Fig. 6b). The spectra for day 222.4 clearly stand out above the adjoining spectra for $\omega/N > 2$. For each drift, the acceleration spectrum is predicted from ε assuming a Froude number $\omega_0/N = 0.5$ (Lien and D'Asaro 2006) and plotted in Fig. 6b as a dashed line. The predicted spectrum matches the measured spectrum well on day 222.4, implying that the two independent diffusivity estimates $\mathcal{D}_\varepsilon$ (Eq. 18) and $\mathcal{D}_\chi$ (Eq. 22) are nearly the same. At the other times, the measured spectrum is dominated by pressure sensor noise (black dashed line) and internal waves, with the predicted turbulent signal falling far below these. Only the $\mathcal{D}_\chi$ estimate is useful.

Figure 6c,d shows the pressure, σ, and Π variations for the three drift segments centered on the event. Before and after the event, the float remains within 0.03 kg m^{-3} of the target isopycnal and Π varies by less than 0.01 kg m^{-3} from its average value in each drift. At about day 222.31 the measured density rapidly decreases by about 0.1 kg m^{-3}, corresponding to a diapycnal displacement of about 5 m upward (Fig. 5b) and then returns to the target isopycnal over the next 2.5 h. The value of Π similarly increases, but does not return to its initial value, instead settling at a value about 0.04 kg m^{-3} higher. This results in an obviously positive value of Π_t shown, for this drift segment, by the dashed line.

Figure 6e shows $\Pi(\sigma)$ and the polynomial fit over 0.3 kg m^{-3} used to estimate $\Pi_{\sigma\sigma}$. Figure 6f shows the resulting budget of Π_t, as in Fig. 5g. The measured value of Π_t (black) agrees with that estimated (colors) from Eq. 23 within the errors.

These data are interpreted as follows: The water parcel tracked by the float is entrained into the bottom of a 5–10-m thick mixing patch at about day 222.31. The simulation of D'Asaro et al. (2004), their fig. 3c, shows the Lagrangian view of a similar event. Because the mixing patch lies above the float's initial isopycnal σ_0, the mixed water is both lighter and has a higher Π than that initially at σ_0. Because the float is programmed to be isopycnal, it sinks back to σ_0 over the few hours after entrainment, but remains within the patch of mixed, higher-Π water. The presence of an organized packet of internal waves starting at day 222.4 suggests a larger structure associated with the mixing event. Otherwise no explanation of its cause is presented here.

The chlorophyll budget—Figure 7 shows a similar analysis for chlorophyll using the diagnostic equation

$$Chl_t = \frac{\chi}{2} Chl_{\sigma\sigma} \tag{28}$$

Estimates of $Chl_{\sigma\sigma}$ and χ are computed as described above for Π. The observed rate of change on an isopycnal (left in equation, black in Fig. 7e) is compared with that expected from diapycnal diffusivity alone (right in equation, colored in Fig. 7e). The agreement is poor, indicating that Eq. 28 does not apply and that factors other than diapycnal mixing are important in changing the chlorophyll concentration.

Figure 7d compares the chlorophyll measured by the floats (green circles, only every 10th plotted) with the cumulative change in chloropyll from the drift segments only (black). For example, near day 220 the green dots show chlorophyll levels decreasing past 5 mg m^{-3}, corresponding to the contoured levels in Fig. 7a,b at the float (yellow). However, the trends during each drift are increasing (red lines) so that the cumulative change during drifts (black line, 'Lagrangian Change') indicates an increasing chlorophyll during the drifts even though the measured chlorophyll is overall decreasing with time. This difference is explained by the large decreases that occur between drifts. During the profiles and surfacing the float is moved horizontally relative to the target isopycnal so when it again settles onto the isopycnal, it is at a different location and measures a different, and in this case decreased, value of chlorophyll. These changes do not represent changes following the water, rather they show the presence of spatial gradients. It is the Lagrangian changes,

←

Fig. 5. Computation of the diapycnal budget of spice Π. (a) Float trajectory. Drifts are black, profiles are red. (b) Displacement of float from target isopycnal $\sigma_0 = 25.5$ kg m^{-3} during drifts (yellow), map of spice Π around σ_0 (color, black solid line contours), position of isopycnals above and below σ_0 (white lines) by 0.2, 0.3, and 0.4 kg m^{-3}. (c) Stratification at float computed for each drift (solid line) and averaged over about 1.8 d (dashed line). (d) Rate of change of spice at σ_0 averaged as in panel c corrected for solar heating (black solid line) and uncorrected for solar heating (pink solid line). Vertical bars show 1 and 2 SD of error. (e) Second derivative of spice with respect to potential density $\Pi_{\sigma\sigma}$ computed over three ranges in $\Delta\sigma$ as indicated by the line colors. Dashed lines are computed over two drift segments; solid lines are averaged over 1.8 d. Vertical bars show 1 and 2 SE. (f) Dissipation rate of potential density variance (black solid line) computed using Eq. 20. Diapycnal diffusivity (blue solid line) computed from χ using Eq. 8. Both are averaged over 1.8 d. Vertical lines are 68% and 95% confidence limits of the fits. (g) Test of diapycnal balance using Eq. 23. Π_t from panel d (black solid line) is compared with $\chi/2\Pi_{\sigma\sigma}$ (colored lines) from panels e and f adjusted to increase the value of β_s to 1.0 from the nominal 0.6. Vertical bars are 1 SE. All plots in panel g were also computed using a linearized version of Π and plotted in panel g as light lines of the same color slightly offset in time. This is most apparent on the red lines near day 210.

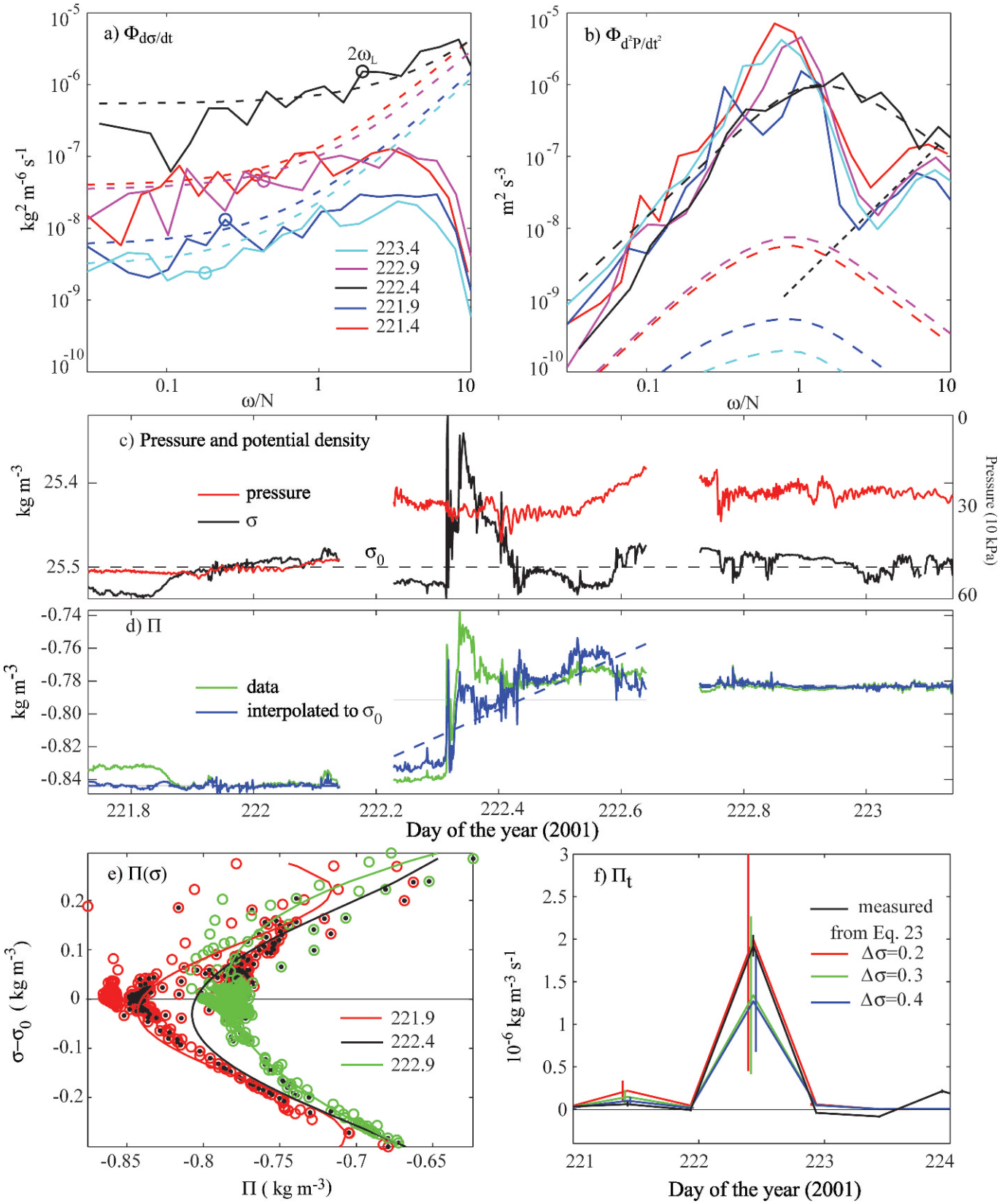

Fig. 6. Detailed view of the intense mixing event on day 222. (a) Spectra of potential density change for the intense mixing drift (black) and surrounding drifts (colored). Model spectra (dashed line) are fit for $\omega < 2\omega_L$. The value of ω_L is indicated by the heavy circles. (b) Spectra of vertical acceleration for the event drift (black) and surrounding drifts (colored). Model acceleration spectra (dashed lines) with ε computed from the density spectra. (c) Time series of depth and σ for the event drift and the drifts preceding and following it. (d) Time series of spice Π for these three drifts. (e) Π as a function of σ for these three drifts (dots and circles) and quartic fits to these (lines). (f) Spice budget for the 3 d centered on the event as in Fig. 5g.

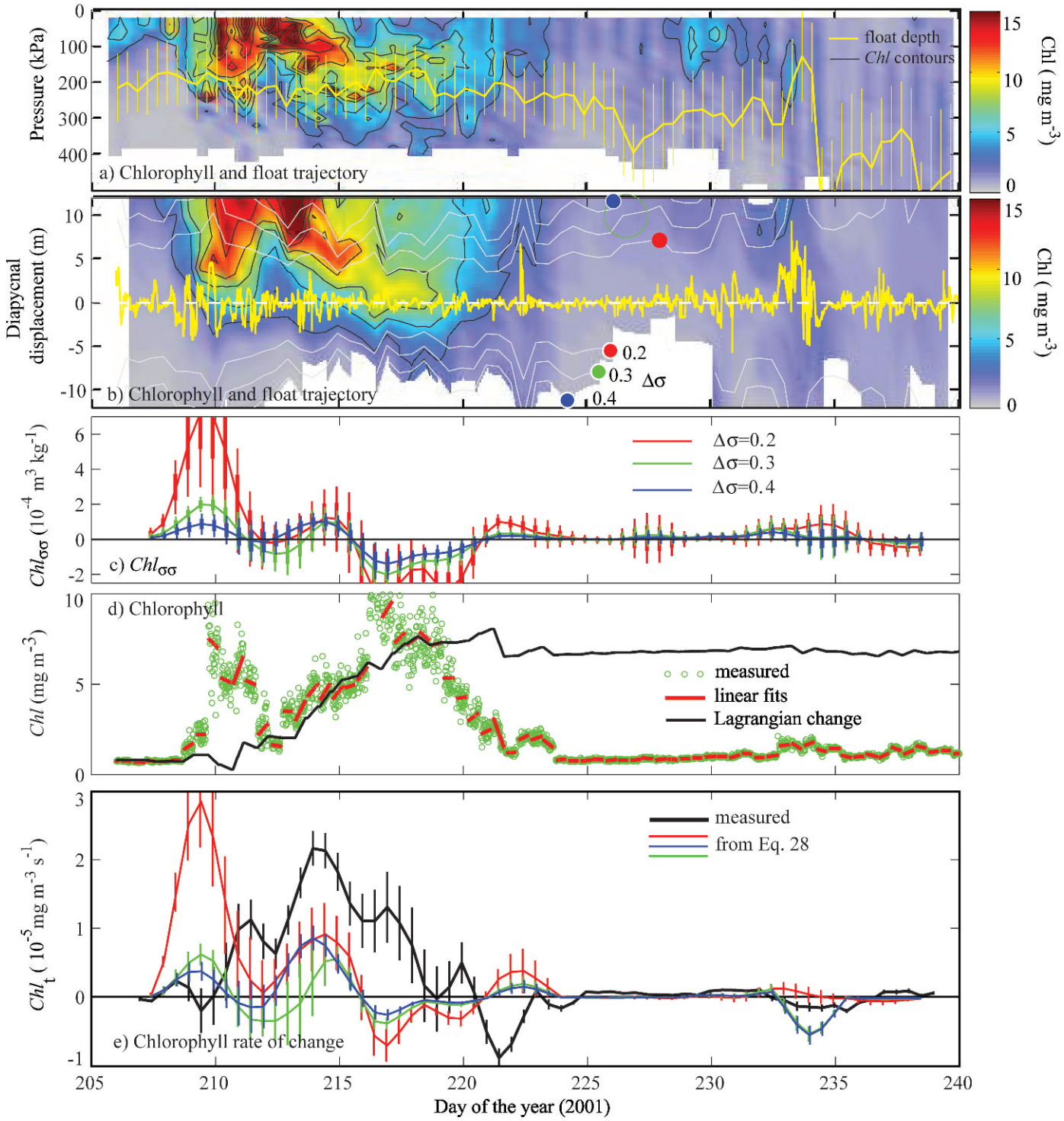

Fig. 7. The diapycnal budget of chlorophyll. (a) Color map and contours of chlorophyll *Chl* from profiles, overlaid by the float trajectory (yellow) shown as mean and standard deviation of depth for each drift segment. (b) Color map, contours, and float trajectory as in panel a but relative to the target isopycnal $\sigma_0 = 25.5$ kg m^{-3}. Positions of isopycnals 0.2, 0.3 and 0.4 kg m^{-3} above and below σ_0 (white lines). (c) Second derivative of chlorophyll $Chl_{\sigma\sigma}$ computed over three ranges of $\Delta\sigma$ as indicated by the line colors and averaged over 1.8 d. Vertical bars show 1 and 2 SE. (d) Chlorophyll during the float drifts (green dots, only every 10th shown), linear fits to these as in Fig. 4 (red lines). Cumulative Lagrangian change (black line) created by placing the red lines end to end. (e) Test of diapycnal balance using Eq. 28. Rate of change of chlorophyll, Chl_t, averaged over 1.8 d (black) is compared with $\chi/2\Pi_{\sigma\sigma}$ (colored lines) similarly averaged. The value of β_s has been increased to 1.0 from the nominal 0.6. Vertical bars are 1 SE.

the cumulative changes during the float drifts, that represent true temporal changes following the water. It is these, black in Fig. 7d,e, that do not agree with the predictions of Eq. 28 in Fig. 7e.

Interpretation

Figure 5g provides a quantitative test of whether spice, and thus implicitly temperature and salinity, are governed by the diffusion equation

$$\frac{D\Pi}{Dt} = \mathcal{D}\frac{\partial^2\Pi}{\partial d} + Q^{\Pi} \tag{29}$$

where the time derivative is taken in a water-following (Lagrangian) frame and the d derivative is taken perpendicular to the isopycnal. The differences between Eqs. 29 and 23 or 12 result from the latter two being set in the more computationally convenient isopycnal frame rather than Langrangian frame. The test applies for measurements averaged over several meters and several days.

If Eq. 29 is not true, there are several possibilities. First, and most likely, isopycnal diffusion is important. Other possibilities include different diffusivities for temperature and salinity (McDougall 1984) or possibly unknown errors in the computation.

Figure 5g shows regions where diapycnal mixing dominates and regions where it does not. The clearest diapycnal case occurs on day 222 (the first vertical yellow bar) and is described in great detail above. The clearest nondiapycnal region is before day 210. Here $\Pi_{\sigma\sigma}$ is clearly positive and χ is large, yet Π_t is nearly zero, suggesting that the tendency for diapycnal mixing to decrease Π is roughly balanced by other processes, presumably isopycnal mixing. The periods of very low mixing on days 219 and 224–227 do not show a diapycnal balance. However, χ is so small that it is not clear that the inertial subrange methods are accurate here.

The most interesting period is associated with the rapid increase in Π on days 232–235 (the second vertical yellow bar). This change most likely represents the float crossing the front between subpolar and subtropical waters. A front is evident in satellite sea surface temperature images near the float's location at this time. However, because the float's location is poorly known, its trajectory relative to this front cannot be determined. The float's isopycnal rises to the surface on the low Π (cold) side of the front, and then plunges to about 50-m depth on the high Π (warm) side. The float itself makes this transition during a downward profile, not during a drift, so that the transition is not Lagrangian and does not necessarily represent the path by which water crosses the front. As the float approaches the front, the layer of low Π water becomes increasingly thin and $\Pi_{\sigma\sigma}$ increases. The mixing balance remains nearly diapycnal, with Π_t also increasing until day 233. As the float's isopycnal surfaces and plunges $\Pi_{\sigma\sigma}$ switches sign, χ increases, yet Π_t remains positive. At the front, therefore, a diapycnal balance no longer holds, despite strong diapycnal mixing, suggesting that isopycnal mixing is dominant for this short period as also reported by Alford et al. (2005). The strong mixing also implies a strong diapycnal velocity, estimated at a few millimeters per second, comparable with those measured by Barth et al. (2004) in a similar environment.

The chlorophyll budget (Fig. 7e) is dominated by a bloom extending from days 210 to 225. The float skirted the lower edge of this bloom. As discussed above, the Lagrangian changes within each drift are different from the changes following the float. The Lagrangian changes (Fig. 7d, heavy black line) show an increase to about 7 mg m^{-3} in 10 d with no changes thereafter. The measured chlorophyll increases irregularly to the same value and then decreases to almost zero in about 5 d. This latter decrease must represent a spatial gradient in chlorophyll. Detailed SeaSoar surveys in this same region (O'Malley et al. 2002) just after the float's transit show a similar bloom, with its outer edge corresponding roughly to the isobath of the float (70–100 m). The gradient at the outer edge is strong, with 7 mg m^{-3} change occurring in about 5 km. Unfortunately, the failure of GPS measurements on this float prevents an accurate measurement of the surface currents and thus the deviation of its track from the water motion on its isopycnal. However, D'Asaro (2004) estimates drifts for float 10, which followed approximately the same track, as roughly 1 km d^{-1} during this time. It is thus reasonable that the float traveled just below and just to the west of this bloom, in a region of strong isopycnal and diapycnal gradients in chlorophyll.

The dominant feature of the Lagrangian chlorophyll change Chl_t (Fig. 7e) is the increase in chlorophyll as the float enters the bloom. This is not explained by diapycnal diffusion. Could it be due to phytoplankton growth? Light levels at the float are low; the average downward irradiance from days 210 to 220 is about 2 W m^{-2} at the float. Using the parameters from Spitz et al. (2003) for light-limited growth, this would correspond to an e-folding time of 20 d compared with the observed growth rate (Chl_t/Chl) of about 4 d. Growth could play a role, particularly if the phytoplankton at this depth were highly light adapted. However, given the strong correspondence between the observed increase at the float and the presence of the bloom above the float, transport is a more likely explanation. Sinking of a few meters per day of phytoplankton could also easily explain the observed increase at the float. The pattern of chlorophyll on days 213–218 suggests this. Equally likely is isopycnal mixing across the strong isopycnal gradients. Using an isopycnal diffusivity of 4 m^2 s^{-1} measured in this area (Dale et al. 2006) and a plausible $\nabla^2 Chl$ = 7 mg m^{-3} / (1,000 m)^2 yields $Chl_t = 1.2 \times 10^{-5}$ mg m^{-3} s^{-1}, comparable with the observations.

Large errors in the second derivatives $\Pi_{\sigma\sigma}$ and $Chl_{\sigma\sigma}$ are major weaknesses in this analysis. The use of well-calibrated pairs of CTD sensors on the floats, as commonly done in other deployments, would help significantly. The other major weakness is the lack of horizontal measurements to define isopycnal processes. Mapping measurements around a drifting float, similar to those made by Barth et al. (2004), is the most obvious approach.

Data from an isopycnal-following float were used to investigate the relative importance of diapycnal and isopycnal mixing in changing water properties. An expression for the rate of change of a scalar measured along an

isopycnal trajectory due to diffusion and requiring only diapycnal derivatives was derived following McDougall (1984). The diapycnal diffusivity was estimated from the spectrum of potential density at frequencies above N (D'Asaro and Lien 2007). Together, these form a test Eq. 23 for a purely diapycnal mixing balance.

This test was applied to two scalars, spice (Flament 2002), a convenient combination of temperature and salinity, and chlorophyll. Both were measured for 35 d by a float tracking a mid-depth isopycnal on the Oregon shelf. Time series of Π and *Chl* on the isopycnal were constructed by correcting for the small diapycnal motion of the float. The diapycnal derivatives were estimated from the float data near the isopycnal. A bio-optical model was used to calibrate chlorophyll and to derive the local rate of solar heating from measurements of downwelling radiation at 490 nm on the float. Independent tests of whether the observed rates of change were due only to diapycnal diffusivity were generated every 1.8 d. The following conclusions about mixing apply to averages of these data of about 1.8 d in time and about 10 m in the vertical.

Variations in spice, and by inference temperature and salinity, were primarily due to diapycnal mixing, most spectacularly in a single large mixing event. The observed diapycnal balance could only be made to work on average, however, by postulating a factor of 1.6 change in the D'Asaro and Lien (2007) estimate of the appropriate Kolomogorov constant. Although this change is within the uncertainty of their estimate and perhaps subject to additional biases, it emphasizes the continued need to refine such estimates.

At times, a diapycnal balance did not apply to spice and, by inference, isopycnal mixing must have been important. Variations in chlorophyll rarely obeyed a diapycnal balance. Instead, some unknown combination of biological growth, planktonic sinking across the strong vertical gradients, or isopycnal mixing across the strong isopycnal gradients must have dominated. The observed difference between the behavior of a physical and biological variable may be coincidence; the time series are not long enough to justify a more general conclusion.

These data clearly show a high degree of variability in diapycnal mixing in the thermocline over the Oregon shelf, even when averaged over several days (e.g., Fig. 5f). This is consistent with previous measurements (Gregg et al. 1993; Moum and Nash 2000). They also suggest that the balance between isopycnal and diapycnal mixing may be equally variable, with isopycnal effects perhaps concentrated at fronts, and with the relative importance of isopycnal and diapycnal effects for scalar mixing highly dependent on the distribution of the scalar.

References

Alford, M., M. Gregg, and E. A. D'Asaro. 2005. Mixing, 3-d mapping and lagrangian evolution of a thermohaline intrusion. J. Phys. Oceanogr. **35:** 1689–1711.

Barth, J. A., D. Hebert, A. Dale, and D. S. Ullman. 2004. Direct observations of along-isopycnal upwelling and diapycnal velocity at a shelfbreak front. J. Phys. Oceanogr. **34:** 543–565.

Boyd, T., M. D. Levine, P. M. Kosro, S. R. Gard, and W. Waldorf. 2002. Observations from moorings on the oregon continental shelf, May–August 2001. Data report 190 COAS reference 2002-6, Oregon State University, College of Ocean and Atmospheric Sciences, Corvallis, Oregon.

Dale, A. C., M. D. Levine, J. A. Barth, and J. A. Austin. 2006. A dye tracer reveals cross-shelf dispersion and interleaving on the Oregon shelf. Geophys. Res. Lett. **33:** 4.

D'Asaro, E. 2007. Solar power for autonomous floats. J. Atmos. Ocean. Technol. **24:** 1309–1314.

———, and R. Lien. 2007. Measurement of scalar variance dissipation from Lagrangian floats. J. Phys. Oceanogr. **24:** 1066–1077.

———, R. Lien, and F. Henyey. 2007. High-frequency internal waves on the Oregon continental shelf. J. Phys. Oceanogr. **37:** 1956–1967.

D'Asaro, E. A. 2003. Performance of autonomous Lagrangian floats. J. Atmos. Ocean. Technol. **20:** 896–911.

———2004. Lagrangian trajectories on the Oregon shelf during upwelling. Cont. Shelf Res. **24:** 1421–1436.

———, K. B. Winters, and R. C. Lien. 2004. Lagrangian estimates of diapycnal mixing in a simulated K-H instability. J. Phys. Oceanogr. **21:** 799–809.

Flament, P. 2002. A state variable for characterizing water masses and their diffusive stability: Spiciness. Prog. Oceanogr. **54:** 493–501.

Gregg, M. 1987. Diapycnal mixing in the thermocline: A review. J. Geophys. Res. **92:** 5249–5286.

Gregg, M. C., H. E. Seim, and D. B. Percival. 1993. Statistics of shear and turbulent dissipation profiles in random internal wave fields. J. Phys. Oceanogr. **23:** 1777–1799.

Jerlov, N. G. 1976. Marine optics. Elsevier.

Jin, Z., T. P. Charlock, K. Rutledge, K. Stamnes, and Y. Wang. 2006. Analytical solution of radiative transfer in the coupled atmosphere–ocean system with a rough surface. Appl. Opt. **45:** 7443–7455.

Lien, R. C., and E. A. D'Asaro. 2006. Measurement of turbulent kinetic energy dissipation rate with a Lagrangian float. J. Atmos. Ocean. Technol. **23:** 964–976.

———, E. A. D'Asaro, and G. T. Dairiki. 1998. Lagrangian frequency spectra of vertical velocity and vorticity in high-Reynolds number oceanic turbulence. J. Fluid Mech. **362:** 177–198.

McDougall, T. J. 1984. The relative roles of diapycnal and isopycnal mixing on subsurface water mass conversion. J. Phys. Oceanogr. **14:** 1577–1589.

Morel, A., and D. Antoine. 1994. Heating rate within the upper ocean and its relation to its bio-optical state. J. Phys. Oceanogr. **24:** 1652–1665.

———, and S. Maritorena. 2001. Bio-optical properties of oceanic waters: A reappraisal. J. Geophys. Res. **106:** 7163–7180.

Moum, N., and J. Nash. 2000. Topographically induced drag and mixing at a small bank on the continental shelf. J. Phys. Oceanogr. **30:** 2049–2054.

O'Malley, R., J. A. Barth, and A. Y. Erofeev. 2002. Seasoar observations during the coastal ocean advances in shelf transport (COAST) survey II, W0108A, 6-25 August 2001.Data report 186, reference 2002-2, College of Oceanic and Atmospheric Sciences, Oregon State University, Corvallis, Oregon.

Osborn, T. R. 1980. Estimates of the local rate of vertical diffusion from dissipation measurements. J. Phys. Oceanogr. **10:** 83–89.

———, and C. S. Cox. 1972. Oceanic fine structure. Geophys. Fluid Dyn. **3:** 321–345.

Spitz, Y. H., P. Newberger, and J. S. Allen. 2003. Ecosystem response to upwelling off the Oregon coast: Behavior of three nitrogen-based models. J. Geophys. Res. **108:** 7–22.
Sreenivasan, K. 1996. The passive scalar spectrum and the Obukov–Corrsin constant. Phys. Fluids **8:** 189.
Sundermeyer, M. A., and J. F. Price. 1998. Lateral mixing and the North Atlantic Tracer Release Experiment: Observations and numerical simulations of Lagrangian particles and a passive tracer. J. Geophys. Res. **103:** 21481–21497.
Thorpe, S. A. 2005. The turbulent ocean. Cambridge.
Winters, K. B., and E. A. D'Asaro. 1996. Diapycnal fluxes in density stratified flows. J. Fluid Mech. **317:** 179–193.

Received: 20 September 2007
Accepted: 10 January 2008
Amended: 19 February 2008